The Astrophysical Journal, 872:62 (12pp), 2019 February 10 https://doi.org/10.3847/1538-4357/aafbe8

Turbulent Dynamo in a Weakly Ionized Medium

Siyao Xu[1,3], Sudip K. Garain[2], Dinshaw S. Balsara[2], and A. Lazarian[1]
[1] Department of Astronomy, University of Wisconsin, 475 North Charter Street, Madison, WI 53706, USA; sxu93@wisc.edu, lazarian@astro.wisc.edu
[2] Department of Physics, University of Notre Dame, Notre Dame, IN 46556, USA; sgarain@nd.edu, dbalsara@nd.edu
Received 2018 September 12; revised 2019 January 1; accepted 2019 January 2; published 2019 February 11

Abstract

The small-scale turbulent dynamo is an important process contributing to the cosmic magnetization. In partially ionized astrophysical plasmas, the dynamo growth of magnetic energy strongly depends on the coupling state between ions and neutrals and the ion-neutral collisional damping effect. A new damping stage of turbulent dynamo in a weakly ionized medium was theoretically predicted by Xu & Lazarian. By carrying out a 3D two-fluid dynamo simulation, we have for the first time numerically confirmed the physical conditions and the linear-in-time growth of the magnetic field strength of the damping stage of a dynamo. The dynamo-amplified magnetic field has a characteristic length as the damping scale, which increases with time and can reach the injection scale of turbulence after around eight turnover times of the largest eddy, given sufficiently low ionization fraction and a weak initial magnetic field. Due to the weak coupling between ions and neutrals, most turbulent energy carried by neutrals cannot be converted to magnetic energy, resulting in a relatively weak magnetic field at the end of the dynamo. This result has important implications for the growth of magnetic fields in the partially ionized interstellar medium and shock acceleration of Galactic cosmic rays.

Key words: dynamo – ISM: magnetic fields – turbulence

1. Introduction

Magnetic fields pervade the universe and are manifest in diverse astrophysical systems (Han 2017). The turbulent dynamo, which both amplifies the strength of the magnetic field and increases its coherence length, is the most promising mechanism to account for the growth and maintenance of cosmic magnetism (Brandenburg & Subramanian 2005). In particular, the turbulent dynamo acting on scales comparable or smaller than the driving scale of turbulence, i.e., the small-scale dynamo, is much more efficient than the large-scale dynamo, and also more generally operates in astrophysical environments wherever the turbulent energy exceeds the magnetic energy.

Depending on the physical conditions, there are a variety of dynamo regimes (Xu & Lazarian 2016, hereafter XL16). In the case of a large Prandtl number, which is the ratio of viscosity to resistivity, the kinematic regime of the small-scale dynamo at sub-viscous scales has been extensively studied (e.g., Maron & Blackman 2002; Schekochihin et al. 2002; Maron et al. 2004). The concentration of the magnetic energy at the small resistive scale claimed in these theoretical and low-resolution numerical studies was disproved by high-resolution dynamo simulations (Haugen et al. 2004).[4] Meanwhile, the nonlinear regime of the small-scale dynamo in the inertial range of turbulence has also been studied numerically (Cho & Vishniac 2000; Cho et al. 2009; Beresnyak 2012), which is found to be characterized by a very inefficient linear-in-time growth of magnetic energy. Recent theoretical and numerical advances in the study of magnetohydrodynamic (MHD) turbulence (Goldreich & Sridhar 1995; Lazarian & Vishniac 1999; Maron & Goldreich 2001; Cho et al. 2002b; Kowal et al. 2009, 2012) enable us to construct an analytical theory of the nonlinear turbulent dynamo (XL16), which has been shown to be in quantitative agreement with numerical measurements. In XL16, the turbulent diffusion of magnetic fields enabled by the turbulent magnetic reconnection (Lazarian & Vishniac 1999) was identified as the physical origin of the low efficiency of the nonlinear dynamo. Additionally, XL16 also analytically discovered a transitional stage connecting the kinematic and nonlinear regimes, where the peak of the magnetic energy spectrum shifts from the resistive scale to the viscous scale. Their theoretical prediction on the sub-viscous spectral tail k^{-1} formed during the transitional stage is consistent with the numerical result in Haugen et al. (2004).

In astrophysical plasmas with a significant neutral component in, e.g., the early universe, cold phases of the interstellar medium (ISM), protoplanetary disks, and the solar chromosphere, both MHD turbulence and turbulent dynamo are influenced by partial ionization (Xu & Lazarian 2017b). Ion-neutral collisional damping of linear MHD waves has been earlier studied by, e.g., Langer (1978), Balsara (1996), Zaqarashvili et al. (2011). On the basis of the updated understanding of MHD turbulence mentioned above, the damping of MHD turbulence due to ion-neutral collisions and the viscosity in neutrals has been studied both analytically (Lithwick & Goldreich 2001; Lazarian et al. 2004; Xu et al. 2015, 2016; Xu & Lazarian 2017b) and numerically (Tilley & Balsara 2008, 2010, 2011; Downes 2012; Meyer et al. 2014; Burkhart et al. 2015).

Regarding the small-scale dynamo in a partially ionized medium, the damping effect due to ion-neutral collisions on the efficiency of the dynamo has been discussed in, e.g., Kulsrud & Anderson (1992), and Subramanian (1998). The new findings in XL16 include (i) a sub-viscous spectral tail k^{-1} formed during the transitional stage at a relatively high ionization fraction; (ii) a damping stage of a dynamo characterized by a linear-in-time growth of magnetic field strength at a relatively low ionization fraction; (iii) the nonlinear stage of a dynamo with a universal dynamo efficiency irrespective of the ionization fraction; and (iv) a direct relation of the damping

[3] Hubble Fellow.
[4] In fact, after a close inspection of, e.g., Figure 1 of Maron & Blackman (2002; as pointed out by Haugen et al. 2003) and Figure 12 in Maron et al. (2004), one can easily see that their results also show the peak scale of the magnetic energy spectrum to be significantly distant from the resistive scale.

of MHD turbulence to that of the turbulent dynamo. These theoretical findings have also been applied to studying the role of magnetic fields in, e.g., star formation in the early universe (XL16) and cosmic-ray acceleration at shocks (Xu & Lazarian 2017a, hereafter XL17),

In this work, our purpose is to numerically test the damping stage of a dynamo in a weakly ionized medium. Differing from the exponential growth of magnetic energy in the sub-viscous range (Kulsrud & Anderson 1992), XL16 demonstrated that the damping stage of the dynamo takes place within the inertial range of turbulence. It arises at a sufficiently low ionization fraction such that (a) ions and neutrals are only weakly coupled, and thus most turbulent energy in neutrals is not involved in the dynamo; (b) the ion-neutral collisional damping scale coincides with the dynamo driving scale; (c) the magnetic field strength grows linearly with time; and (d) there is no equipartition between the turbulent and magnetic energies. We will present the first numerical test of the theoretical prediction on the damping stage of a dynamo in XL16 by carrying out a 3D two-fluid numerical simulation. We use the two-fluid version of the RIEMANN code (Balsara 1998a, 1998b, 2004, 2010, 2012; Balsara & Spicer 1999a, 1999b) to simulate the weakly ionized turbulent plasma. The RIEMANN code has been widely used for studying astrophysical problems in partially ionized plasmas (e.g., Tilley & Balsara 2010, 2011; Meyer et al. 2014). In general, a two-fluid MHD simulation requires extensive computational effort. Our two-fluid dynamo simulation is even more challenging in order to achieve (i) a low ionization fraction to ensure the emergence of the damping stage; (ii) a large inertial range as the damping scale increases with time; and (iii) a long simulation time to observe the entire dynamo evolution of magnetic fields. Despite its high computational cost, this numerical testing will provide direct evidence for the XL16 theory of the damping stage of the dynamo and quantitatively reinforce our understanding of the dynamo physics in a weakly ionized medium. It is also important for further applications of the theory to studying the evolution and structure of magnetic fields in neutral-dominated astrophysical environments.

The paper is organized as follows. In Section 2, we describe the physical conditions and the analytically derived evolution law of the magnetic field for the damping stage of a dynamo. In Section 3, we present the numerical results of the two-fluid simulation and their comparisons with our theoretical predictions. In Section 4, we further examine the importance of the damping stage of a dynamo in the partially ionized ISM. A discussion of the effect of ion-neutral coupling on MHD turbulence and a turbulent dynamo is in Section 5. A summary follows in Section 6.

2. Damping Stage of a Dynamo in a Weakly Ionized Medium

By stretching magnetic field lines, turbulent motions can amplify magnetic fields. Meanwhile, magnetic fields also undergo diffusion due to plasma or/and turbulence effects. These two opposing processes, turbulence stretching and magnetic field diffusion, together determine the dynamo efficiency.

In the kinematic dynamo regime, the magnetic energy is lower than the turbulent energy, and the magnetic field is dynamically unimportant. The diffusion only arises from plasma effects. In the case of a weakly ionized plasma, i.e., molecular clouds in the ISM, the diffusion in the kinematic dynamo regime mainly comes from the slippage between ions and neutrals. So the ion-neutral collisional damping is the dominant damping process of magnetic fluctuations, whereas other damping effects, including viscous damping and resistive damping, are negligible (Kulsrud & Anderson 1992; Xu et al. 2016).

Here, we consider the damping stage of a dynamo in a weakly ionized medium, which was first identified by XL16. It is in the kinematic regime and subjected to severe ion-neutral collisional damping.

2.1. Physical Conditions for the Damping Stage of a Dynamo

Depending on the ionization fraction, the turbulent dynamo in a partially ionized medium undergoes different evolutionary stages. To observe a significant damping effect on the dynamo growth of magnetic energy in a damping stage, the ionization fraction should be sufficiently small, such that the ion-neutral coupling is weak and the ion-neutral collisional damping is strong. We note that unlike the strongly coupled regime where ions and neutrals are strongly coupled together and the decoupled regime where the two species are decoupled from each other, in the weakly coupled regime considered here, neutrals are decoupled from ions, but ions can still collide with surrounding neutrals in a weakly ionized medium, thus the motions of ions and magnetic fields are more severely damped (Xu et al. 2016). Next, we detail the physical conditions for the damping stage of a dynamo to arise.

Condition (1): a sufficiently small ionization fraction.

The damping stage of a dynamo is characterized by the weak coupling state between ions and neutrals and the consequent severe ion-neutral collisional damping. Quantitatively, the neutral-ion collisional frequency ν_{ni} should be smaller than the dynamo stretching rate Γ_l of magnetic fields to ensure the weak coupling between ions and neutrals (see Table 1 for the main notations used in this paper). The former is given by $\nu_{ni} = \gamma_d \rho_i$, with the drag coefficient γ_d (see, e.g., Shu 1992) and the ion density ρ_i. The latter is determined by the turbulence eddy-turnover rate v_l/l, where v_l is the turbulent velocity at the length scale l. According to the Kolmogorov scaling of hydrodynamic turbulence, v_l decreases with l as

$$v_l = V_L \left(\frac{l}{L}\right)^{\frac{1}{3}} \tag{1}$$

along the turbulent energy cascade, where V_L is the turbulent velocity at the injection scale L of turbulence. It can be easily seen that smaller eddies have larger eddy-turnover rates. Since the eddies at the ion-neutral collisional damping scale l_d of magnetic fluctuations are the smallest ones that can effectively stretch magnetic field lines, they are mainly responsible for the dynamo action. The corresponding dynamo stretching rate is $\Gamma_d = v_d/l_d$, where v_d is the turbulent velocity at l_d.

The above condition is formulated as (XL17)

$$\frac{2}{\mathcal{C}\Gamma_d} < 1, \tag{2}$$

Table 1
List of Main Notations

Description	Symbol
magnetic energy	$\mathcal{E}_M$
magnetic energy spectrum	$M(k, t)$
drag coefficient	γ_d
neutral-ion collision frequency	ν_{ni}
ion-neutral collision frequency	ν_{in}
ion-neutral collisional damping scale	l_d
neutral viscosity	ν_n
viscous damping scale	l_ν
peak scale of $M(k, t)$	l_p
injection scale of turbulence	L
turbulent velocity at L	V_L
eddy-turnover time at L	$\tau_{\rm eddy}$
turbulent velocity at l	v_l
stretching rate/turnover rate at length scale l	Γ_l
stretching rate/turnover rate at l_d	Γ_d
stretching rate/turnover rate at l_ν	Γ_ν
stretching rate/turnover rate at L	Γ_L
stretching rate/turnover rate at l_p	Γ_p
ion mass density	ρ_i
neutral mass density	ρ_n
total mass density	ρ
neutral fraction	ξ_n
ion-neutral coupling coefficient	η_c
effective density (Equation (30))	$\rho_{\rm eff}$
Alfvén speed of ionized fluid	V_{Ai}
Alfvén Mach number of ionized fluid	M_{Ai}
Alfvén speed of strongly coupled ions and neutrals	$V_{A,\rm tot}$
Alfv *é*n speed in terms of $\rho_{\rm eff}$	$V_{A,\rm eff}$

where

$$\mathcal{C} = \frac{\xi_n}{3\nu_{ni}} \approx \frac{1}{3\nu_{ni}}, \tag{3}$$

which imposes a constraint on the maximum value of the ionization fraction. We note that the expression on the LHS of Equation (2) is related to the Reynolds number at l_d defined in Balsara (1996). Here, the ratio between the neutral density and the total density $\xi_n = \rho_n/\rho$ is approximately equal to unity in a weakly ionized medium. This implies that when the ionization fraction is sufficiently small, neutrals collide with ions so infrequently that neutrals are basically decoupled from the dynamo-stretched field lines. On the other hand, in a neutral-dominated medium, ions can still collide with surrounding neutrals. Quantitatively, there is $\nu_{in} \gg \Gamma_d$, where $\nu_{in} = \gamma_d \rho_n$ is the ion-neutral collisional frequency. It is related to ν_{ni} by $\nu_{in} = (\rho_n/\rho_i)\ \nu_{ni}$. Evidently, ν_{in} is much larger than ν_{ni} in a weakly ionized medium. Because of the weak coupling between ions and neutrals, the dynamo action cannot effectively convert the turbulent kinetic energy carried by neutrals to the magnetic energy.

Condition (2): sufficiently small magnetic energy.

As mentioned earlier, the magnetic energy in the kinematic dynamo regime is smaller than the turbulent energy. At l_d, where the local turbulent motions dominate the dynamo action, there should be

$$\mathcal{E}_M < \frac{1}{2} v_d^2 \tag{4}$$

where

$$\mathcal{E}_M = \frac{1}{2} V_A^2 \tag{5}$$

is the magnetic energy, and V_A is the Alfvén speed. So the relation in Equation (4) is equivalent to $V_A < v_d$.

Meanwhile, there exists the equalization between Γ_d and the ion-neutral collisional damping rate $\omega_{\rm IN}$ at l_d, where $\omega_{\rm IN}$ is given by (Kulsrud & Anderson 1992)

$$\omega_{\rm IN} = \mathcal{C} l^{-2} \mathcal{E}_M = \frac{\mathcal{C}}{2} l^{-2} V_A^2. \tag{6}$$

From $\Gamma_d = \omega_{\rm IN}$ at l_d, we find

$$l_d = \frac{\mathcal{C}}{2} V_A^2 v_d^{-1}. \tag{7}$$

Combining the above expression with the condition in Equation (2) yields $V_A < v_d$. It shows that under *Condition (1)*, *Condition (2)* is naturally satisfied. In fact, due to the severe damping effect at a small ionization fraction, the equipartition between the magnetic and turbulent energies at l_d cannot be reached. Any further growth of magnetic energy would break the balanced condition $\Gamma_d = \omega_{\rm IN}$ at l_d until the new balance is achieved at a larger l_d. Hence, the dynamo in the damping stage remains in the kinematic regime.

Condition (3): dominant ion-neutral collisional damping over the neutral viscous damping.

As mentioned above, ion-neutral collisional damping is the dominant damping effect for the damping stage of a dynamo. But we note that as the ion-neutral collisional damping depends on the magnetic energy (Equation (6)), to ensure $\omega_{\rm IN} > \omega_{\rm NV}$, where

$$\omega_{\rm NV} = l^{-2} \nu_n, \tag{8}$$

is the damping rate related to the kinematic viscosity ν_n in neutrals, we should have the magnetic energy (Equations (6) and (8))

$$\mathcal{E}_M > \mathcal{C}^{-1} \nu_n. \tag{9}$$

When we consider a small ionization fraction and the dynamo growth of magnetic energy, the above condition can be easily satisfied.

Alternatively, when the ion-neutral collisional damping dominates over the neutral viscous damping, l_d should be larger than the viscous damping scale l_ν. The condition $l_d > l_\nu$ yields (Equation (7))

$$\mathcal{C} \mathcal{E}_M v_d^{-1} > \nu_n v_\nu^{-1}, \tag{10}$$

where the relation $l_\nu^{-2} \nu_n = v_\nu / l_\nu$ is used, and v_ν is the turbulent velocity at l_ν. Since $v_d > v_\nu$, there must be

$$\mathcal{E}_M > \mathcal{C}^{-1} \nu_n, \tag{11}$$

which recovers the condition in Equation (9).

Under the above conditions (Equation (2) and Equation (9)), we expect that the turbulent dynamo in a weakly ionized medium undergoes a damping stage.

2.2. Magnetic Field Evolution During the Damping Stage of a Dynamo

In the damping stage, the time evolution of magnetic fields strongly depends on the ion-neutral collisional damping. As mentioned earlier, the dynamo stretching rate is given by the eddy-turnover rate at l_d,

$$\Gamma_d = \frac{v_d}{l_d} = L^{-\frac{1}{3}} V_L l_d^{-\frac{2}{3}}, \tag{12}$$

where the Kolmogorov scaling in Equation (1) is used. With the same scaling, the expression of l_d in Equation (7) can be rewritten as

$$l_d = \mathcal{C}^{\frac{3}{4}} L^{\frac{1}{4}} V_L^{-\frac{3}{4}} \mathcal{E}_M^{\frac{3}{4}}. \tag{13}$$

The growth of $\mathcal{E}_M$ results in a stronger damping effect and a larger l_d.

The magnetic fluctuations on length scales larger than l_d follow the Kazantsev spectrum (Kazantsev 1968) as a result of the dynamo stretching,

$$M(k, t) = M_1 \exp\left(\frac{3}{4}\int \Gamma_d dt\right)\left(\frac{k}{k_1}\right)^{\frac{3}{2}}, \tag{14}$$

where M_1 is the initial magnetic energy spectrum at some reference wavenumber k_1. The Kazantsev spectrum depends on both wavenumber k and time t. By integrating $M(k, t)$ over k, we can derive $\mathcal{E}_M$ as a function of t,

$$\mathcal{E}_M(t) = \frac{1}{2}\int_0^{k_d} M(k, t) dk. \tag{15}$$

Combining Equations (12)–(15) and after some straightforward algebra, we arrive at (XL16),

$$\sqrt{\mathcal{E}_M} = \sqrt{\mathcal{E}_{M1}} + \frac{3}{23}\mathcal{C}^{-\frac{1}{2}} L^{-\frac{1}{2}} V_L^{\frac{3}{2}} (t - t_1), \tag{16}$$

with the magnetic energy $\mathcal{E}_{M1}$ at the beginning of the damping stage $t = t_1$. As $\sqrt{\mathcal{E}_M} \propto B$, where B is the magnetic field strength, the damping stage of a dynamo is characterized by a linear-in-time growth of B.

From Equations (14) and (15), we find

$$\frac{d \ln \mathcal{E}_M}{dt} \propto \Gamma_d. \tag{17}$$

Here $\Gamma_d \propto \mathcal{E}_M^{-\frac{1}{2}}$ according to Equations (12) and (13), which results from both the equalization $\Gamma_d = \omega_{\rm IN}$ at l_d and the Kolmogorov scaling of turbulence. Therefore, we have $\sqrt{\mathcal{E}_M} \propto t$.

Furthermore, after inserting Equation (16) into (13), we can also derive the time evolution of l_d,

$$l_d = \left(l_{d1}^{\frac{2}{3}} + \frac{3}{23} L^{-\frac{1}{3}} V_L (t - t_1)\right)^{\frac{3}{2}}, \tag{18}$$

with l_{d1} at $t = t_1$. If the damping stage can proceed until l_d increases up to L, *Condition (1)* (Equation (2)) should be satisfied at L, that is,

$$\frac{2L}{\mathcal{C} V_L} < 1. \tag{19}$$

Compared with the general form in Equation (2), the above condition requires a further smaller ionization fraction, so even the largest eddy-turnover time is still smaller than the neutral-ion collisional time. With neutrals decoupled from the dynamo action on all length scales from the initial l_d up to L, this ensures that the dynamo remains in the kinematic damping stage, and the unsaturated magnetic energy at the end of a dynamo mainly comes from the turbulent energy carried by ions.

When $l_d = L$, the corresponding time is (Equation (18)),

$$t(l_d = L) = t_1 + \frac{23}{3} L^{\frac{1}{3}} V_L^{-1} (L^{\frac{2}{3}} - l_{d1}^{\frac{2}{3}}). \tag{20}$$

Given $l_{d1} \ll L$, the entire damping stage of a dynamo lasts for around 7.7 times the largest eddy-turnover time. The magnetic energy reached at $l_d = L$ is (Equation (13)),

$$\mathcal{E}_M(l_d = L) = \mathcal{C}^{-1} L V_L. \tag{21}$$

In the kinematic damping stage, there is

$$\mathcal{E}_M(l_d = L) < \frac{1}{2} V_L^2, \tag{22}$$

which naturally recovers the condition in Equation (19).

3. Numerical Test of the Damping Stage of a Dynamo with a Two-fluid Simulation

To numerically test the above theory for the damping stage of a dynamo, we perform a 3D two-fluid dynamo simulation using the RIEMANN code (Balsara 1998a, 1998b, 2004, 2010, 2012; Balsara & Spicer 1999a, 1999b). The neutral and ionized fluids are separately treated with the isothermal Euler equations and isothermal MHD equations, respectively. Their coupling is described by the ion-neutral friction term, which is introduced using an operator-split method (Tilley & Balsara 2008; Tilley et al. 2012). We solve the following equations (Draine 1986) using the abovementioned code:

$$\begin{aligned}
&\frac{\partial \rho_i}{\partial t} + \nabla \cdot (\rho_i \boldsymbol{v}_i) = 0,\\
&\frac{\partial \boldsymbol{v}_i}{\partial t} + (\boldsymbol{v}_i \cdot \nabla)\boldsymbol{v}_i = -c_s^2 \nabla \ln \rho_i - \frac{1}{4\pi}\boldsymbol{B} \times (\nabla \times \boldsymbol{B})\\
&\quad - \gamma_d \rho_n (\boldsymbol{v}_i - \boldsymbol{v}_n),\\
&\frac{\partial \boldsymbol{B}}{\partial t} = \nabla \times (\boldsymbol{v}_i \times \boldsymbol{B}),\\
&\frac{\partial \rho_n}{\partial t} + \nabla \cdot (\rho_n \boldsymbol{v}_n) = 0,\\
&\frac{\partial \boldsymbol{v}_n}{\partial t} + (\boldsymbol{v}_n \cdot \nabla)\boldsymbol{v}_v = -c_s^2 \nabla \ln \rho_n - \gamma_d \rho_i (\boldsymbol{v}_n - \boldsymbol{v}_i),
\end{aligned} \tag{23}$$

where $\boldsymbol{v_i}$ and $\boldsymbol{v_n}$ are the velocities of the ionized and neutral fluids, and $\boldsymbol{B}$ is the magnetic field. As the time step is restricted by the Alfvén time step for ions, a two-fluid simulation at a low ionization fraction is computationally very expensive. To reduce the computational cost, a "heavy ion approximation" (HIA, Oishi & Mac Low 2006; Li et al. 2008) with artificially decreased ion Alfvén speed and increased ionization fraction is frequently adopted. However, Tilley & Balsara (2010) showed that the HIA can unphysically affect the dissipation

Table 2
Simulation Parameters

R	L	ρ_i/ρ_n	$V_{\rm rms}$	c_s	M_{Ai0}	$\frac{\nu_{ni}}{V_{\rm rms}/L}$
1024^3	512	1.26×10^{-3}	0.2	1	17.7	0.08

characteristics of magnetic fluctuations. It is also possible to numerically investigate the partially ionized magnetized fluids using the single-fluid treatment by adding an additional diffusive term in the induction equation. However, this approach is unable to capture the two-fluid effect in the weakly coupled regime (Balsara 1996; Xu et al. 2016), which is of key importance to study the damping stage of a dynamo considered here. Therefore, we perform a full two-fluid simulation with realistic ion masses to obtain reliable numerical measurements.

3.1. Simulation Setup

We set initially uniform densities of both ions and neutrals, with the neutral density equal to unity. The ions and neutrals have molecular weights as $\mu_i = 29$ amu (corresponding to HCO+) and $\mu_n = 2.3$ amu (corresponding to H_2 and He), respectively, as the mean molecular mass of ions and neutrals in molecular clouds (Shu 1992; Balsara 1996; Tilley & Balsara 2010; Meyer et al. 2014; Burkhart et al. 2015). The RIEMANN code has been used to simulate two-fluid magnetized turbulence with an ionization fraction as low as 10^{-6} (Tilley & Balsara 2008, 2010). Here, we choose a value of 10^{-4}. The initial seed magnetic field for dynamo amplification is uniform (Cho et al. 2009) and aligned along the x-direction. We drive hydrodynamical turbulence in this initial setup. The hydrodynamic turbulence is forced via driving random Gaussian fluctuations in Fourier space, with the driving scale peaked at $k/2\pi = 2$ and spanning $1 \leqslant k/2\pi \leqslant 4$, and an rms velocity of 0.2 times the sound speed. The turbulence becomes statistically steady after around three turnover times of the largest eddy. We continuously drive the turbulence in both ions and neutrals to maintain a constant turbulent energy and a constant rms velocity throughout the simulation. The turbulent energy cascades toward smaller scales and dissipates at the numerical dissipation scale. To ensure a clear separation between the driving scale of turbulence, the ion-neutral collisional damping scale that increases with time, and the numerical dissipation scale of turbulence, our simulation has a high resolution of 1024^3 mesh points. It is performed in a computational domain given by [0, 1] × [0, 1] × [0, 1].

Table 2 lists the numerical resolution (mesh points), the injection scale (mesh points) where most turbulent energy is injected, the ratio between ρ_i and ρ_n, the rms velocity, the sound speed, the initial Alfvén Mach number $M_{Ai0} = V_{\rm rms}/V_{Ai0}$ of the ionized fluid, where $V_{Ai0} = B_0/\sqrt{4\pi\rho_i}$ is the initial Alfvén speed in terms of the initial magnetic field strength B_0 and ion density ρ_i, the ratio between ν_{ni} and the eddy-turnover rate $V_{\rm rms}/L$ at L. The large value of M_{Ai0} shows that the initial magnetic energy contained in the ionized fluid is much smaller than the turbulent energy.

With our focus on the damping stage of a dynamo, we designate the values of the above parameters in the simulation to satisfy the physical conditions presented in Section 2.

Condition (1):

To ensure that the dynamo stage can proceed until $l_d = L$, we have (Equation (3), Equation (19))

$$\frac{2L}{\mathcal{C}V_L} \approx 0.48 < 1, \tag{24}$$

where the values in Table 2 are adopted and we take $V_L = V_{\rm rms}$. It shows that due to the low ionization fraction, neutrals are decoupled from the dynamo action on all length scales.

Condition (2):

We note that *Condition (2)* is naturally fulfilled given *Condition (1)* (see Section 2.1). Due to the low ionization fraction and strong ion-neutral collisional damping, there is no equipartition between magnetic and turbulent energies on all length scales. At the end of the damping stage at $l_d = L$, the unsaturated magnetic energy mainly contained in ions is smaller than the turbulent energy at L.

Condition (3):

The initial magnetic energy contained in ions is

$$\mathcal{E}_{M0} = \frac{1}{2}V_{Ai0}^2. \tag{25}$$

We rewrite Equation (9) in a dimensionless form and find

$$\frac{\mathcal{E}_{M0}}{\mathcal{C}^{-1}\nu_n} = \frac{1}{6}\frac{1}{M_{Ai0}^2}\frac{V_L/L}{\nu_{ni}}\left(\frac{L}{l_\nu}\right)^{\frac{4}{3}} \approx 1.3 > 1, \tag{26}$$

where the viscous scale is

$$l_\nu = L^{\frac{1}{4}}V_L^{-\frac{3}{4}}\nu_n^{\frac{3}{4}}. \tag{27}$$

In our simulation, l_ν is determined by the numerical dissipation scale, which is of the order of 10 mesh points. With the growth of $\mathcal{E}_M$, the ion-neutral collisional damping is the dominant damping effect and *Condition (3)* is satisfied.

3.2. Comparison between Theoretical Predictions and Numerical Measurements

Early in the simulation, before the turbulent energy spectrum is fully developed, due to the turbulent energy cascade from large to small scales, the dynamo stretching scale, which determines the peak scale of the magnetic energy spectrum, shifts toward smaller scales. The initial weak magnetic field leads to the initially weak ion-neutral collisional damping effect. Thus, the dynamo is in the dissipation-free regime, which is characterized by an exponential growth of magnetic energy. A Kazantsev magnetic energy spectrum on scales larger than the peak scale is expected, as seen earlier in one-fluid dynamo simulations (e.g., Haugen et al. 2004; Brandenburg & Subramanian 2005).

With the growth of magnetic energy, the ion-neutral collisional damping becomes important, so that the magnetic energy spectrum peaks and is also damped at l_d. The dynamo enters the damping stage. As analyzed in Section 2.2, we expect that the magnetic field strength grows linearly with time, and the spectral peak at l_d moves toward larger scales.

In Figure 1, we illustrate $M(k)$ in both the dissipation-free stage and the damping stage. As a comparison, the numerically measured $M(k, t)$ at different times are presented in Figure 2(a). As expected, the spectral peak of $M(k, t)$ indeed first shifts to smaller scales and then back to larger scales. The ascending spectral form on large scales is also consistent with the

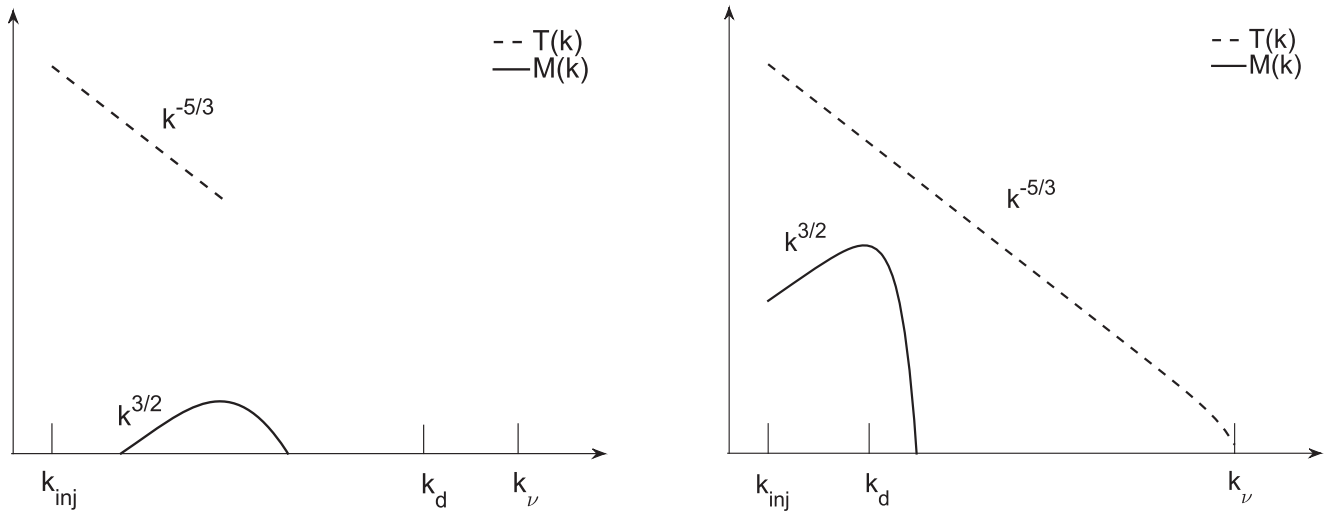

Figure 1. Sketches of the magnetic energy spectrum $M(k)$ and the turbulent kinetic energy spectrum $T(k)$ for the dissipation-free and damping stages of a dynamo, respectively. $k_{\rm inj}$, k_d, and k_ν are the wavenumbers corresponding to L, l_d, and l_ν.

Kazantsev spectrum $\sim k^{3/2}$. Additionally, we also present the stationary and fully developed turbulent energy spectrum $T(K)$, which is expected to follow the Kolmogorov spectrum $k^{-5/3}$. The appearance of a bottleneck effect with a pileup of energy (Falkovich 1994) is observed on small scales of the inertial range, which can be more clearly seen in the compensated turbulent energy spectrum in Figure 2(b).

1. Dissipation-free stage of a dynamo.

When the ion-neutral collisional damping effect is weak, the dynamo stretching leads to an exponential growth of magnetic energy,

$$\mathcal{E}_M = \mathcal{E}_{M0}\exp(2\Gamma_p t). \tag{28}$$

The dynamo growth rate Γ_p corresponds to the eddy-turnover rate at the peak scale l_p of $M(k, t)$. As the spectral peak shifts toward smaller scales, Γ_p increases with time.

To compare with the numerical result, we rewrite Equation (28) in the form

$$\frac{V_{A1,\rm eff}}{V_L} = \frac{V_{A0,\rm eff}}{V_L}\exp\left(\left(\frac{L}{l_p}\right)^{\frac{2}{3}}\frac{t}{\tau_{\rm eddy}}\right), \tag{29}$$

where $\tau_{\rm eddy} = L/V_L$ is the turnover time of the largest eddy at L, and $V_{A0,\rm eff}$ and $V_{A1,\rm eff}$ are the effective Alfvén speeds in terms of the effective density $\rho_{\rm eff}$ at the beginning and the end of the dissipation-free stage. We define $\rho_{\rm eff}$ as

$$\rho_{\rm eff} = \eta_c \rho_i, \tag{30}$$

where η_c is the coupling coefficient, as an indicator of the coupling degree between ions and neutrals. When ions and neutrals are strongly coupled together, there is $\eta_c = \rho/\rho_i$ and $V_{A,\rm eff} = V_{A,\rm tot}$, where $V_{A,\rm tot}$ is the Alfvén speed in terms of the total density. When ions and neutrals are decoupled from each other, we have $\eta_c = 1$ and $V_{A,\rm eff} = V_{Ai}$. Here, we are concerned with the weak coupling regime with $\eta_c \gtrsim 1$, where neutrals are decoupled from ions but ions are still coupled with neutrals. The exact value of η_c will be determined numerically.

By adopting the values in Table 2, we present the above theoretical calculation (Equation (29)) in comparison with the numerical result in Figure 3. Approximately, we use a constant value of $l_p \sim L/3$ as an estimate of the evolving l_p and find

$$\frac{V_{A1,\rm eff}}{V_L} \approx 0.36 \tag{31}$$

at the end of the dissipation-free stage at $t = t_1 = 1.1\tau_{\rm eddy}$.

We stress here that the growth of magnetic energy during the dissipation-free stage indeed enhances the damping effect, but the key and necessary condition for the damping stage to arise is a sufficiently small ionization fraction, i.e., *Condition (1)* (Equation (24)).

2. Damping stage of a dynamo.

We rewrite the evolution law of magnetic energy in the damping stage of a dynamo given by Equation (16) in a dimensionless form

$$\frac{V_{A2,\rm eff}}{V_L} = \frac{V_{A1,\rm eff}}{V_L} + \frac{3\sqrt{2}}{23}\left(\frac{3\nu_{ni}L}{V_L}\right)^{\frac{1}{2}}\frac{(t-t_1)}{\tau_{\rm eddy}}. \tag{32}$$

With the values of parameters in Table 2 used, the theoretical calculation is displayed in Figure 3. By comparing with the numerical measurement, we also found $\eta_c \approx 2.45$. With η_c being of the order of a few, $\rho_{\rm eff}$ is close to ρ_i (Equation (30)). It shows that the growing magnetic energy mainly comes from the turbulent energy contained in ions in the weak coupling regime, as discussed in Section 2.1.

At the end of the damping stage, the theoretical expectation in Equation (21) yields

$$\frac{V_{A2,\rm eff}}{V_L} = \left(6\frac{\nu_{ni}L}{V_L}\right)^{\frac{1}{2}} = 0.69 < 1. \tag{33}$$

The corresponding time is (Equations (31)–(33))

$$t_2 = t_1 + 3.7\tau_{\rm eddy} = 4.8\tau_{\rm eddy}. \tag{34}$$

We see in Figure 3 that the damping stage observed in the numerical simulation is slightly more extended than the above prediction, but the dynamo growth ceases soon after $t = t_2$.

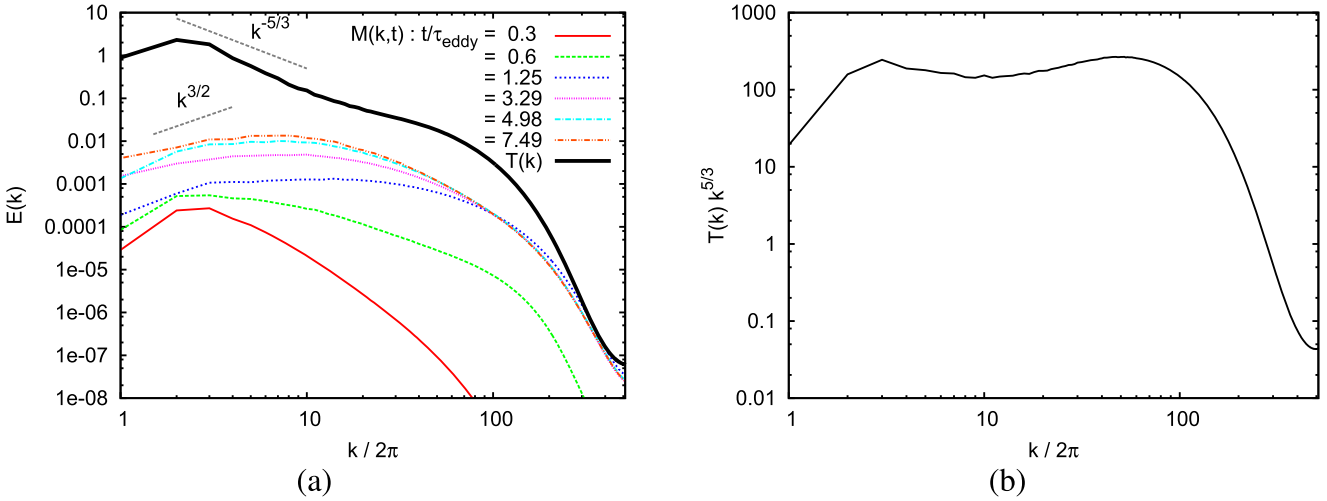

Figure 2. (a) Numerically measured $M(k, t)$ at different times. $T(k)$ is the steady turbulent energy spectrum. The short dashed lines indicate the spectral scalings of the Kazantsev spectrum and Kolmogorov spectrum. (b) Compensated turbulent energy spectrum.

Moreover, the time evolution of l_d in the damping stage is (Equation (18))

$$\frac{l_d}{L} = \left[\left(\frac{l_{d1}}{L}\right)^{\frac{2}{3}} + \frac{3}{23}\frac{(t-t_1)}{\tau_{\rm eddy}}\right]^{\frac{3}{2}}. \quad (35)$$

Starting from (Equations (13) and (31))

$$\frac{l_{d1}}{L} = \left[\frac{V_L}{6\nu_{ni}L}\frac{V_{A1,\rm eff}^2}{V_L^2}\right]^{\frac{3}{4}} = 0.38, \quad (36)$$

we see that l_d reaches L at $t = t_2$ (Equations (34) and (35)). Figure 4 displays the 2D magnetic field structure measured at the end of the simulation, which is dominated by large-scale magnetic field fluctuations. This confirms that the magnetic field resulting from the damping stage of a dynamo has a characteristic length scale comparable to L in our simulation.

4. Physical Conditions in the ISM for the Damping Stage of a Dynamo

As illustrative examples for the applications of the above dynamo theory, here we examine the physical conditions in the partially ionized ISM for the damping stage of a dynamo. Table 3 lists the typical parameters of the warm neutral medium (WNM), the cold neutral medium (CNM), molecular clouds (MC), and dense cores in molecular clouds (DC), where n_H and n_e are the number densities of the atomic hydrogen and electrons, and T is the temperature. Their values are taken from Draine & Lazarian (1998). Additionally, we assume $m_i = m_n = m_{\rm H}$ as the masses of ions and neutrals in WNM and CNM, and $m_i = 29m_{\rm H}$, $m_n = 2.3m_{\rm H}$ in MC and DC (Shu 1992), where $m_{\rm H}$ is the hydrogen atomic mass. We also have $\nu_n = v_{\rm th}/(n_n\sigma_{nn})$, with the neutral thermal speed $v_{\rm th}$, the neutral number density n_n, and the cross section of a neutral-neutral collision $\sigma_{nn} \sim 10^{-14}\,{\rm cm}^2$ (Vranjes & Krstic 2013). The drag coefficient is $\gamma_d = 5.5 \times 10^{14}\,{\rm cm}^3\,{\rm g}^{-1}\,{\rm s}^{-1}$ in WNM and CNM, and $\gamma_d = 3.5 \times 10^{13}\,{\rm cm}^3\,{\rm g}^{-1}\,{\rm s}^{-1}$ in MC and DC (Draine et al. 1983; Shu 1992). We next analyze the turbulent dynamo induced by (a) the globally driven interstellar turbulence and (b) the locally excited turbulence in supernova remnants (SNRs).

(a) Interstellar turbulence.

We consider that the interstellar turbulence driven by supernova explosions has a typical driving condition (Spitzer 1978)

$$L = 30\ {\rm pc},\ \ V_L = 10\ {\rm km\ s}^{-1}. \quad (37)$$

As a result of a turbulent energy cascade, the interstellar turbulence extends from L to l_ν. Here, we assume that the initial seed magnetic field is sufficiently weak, so the turbulent motions on all length scales can contribute to the dynamo growth. In partially ionized phases, to examine *Condition (1)* we calculate the dynamo stretching rate Γ_ν of l_ν-scale eddies and Γ_L of L-scale eddies in comparison with $\mathcal{C}^{-1}$, as presented in Figure 5(a). We find that in WNM and CNM, as *Condition (1)* is not satisfied in the entire inertial range $[L,\ l_\nu]$ of turbulence, the dynamo does not go through the damping stage, but instead has a nonlinear stage (see below). In MC and DC, the damping stage of a dynamo can arise at l_ν, but cannot proceed to L as *Condition (1)* at L is not met. Therefore, the dynamo has both damping and nonlinear stages.

The critical damping scale where the damping stage terminates can be determined by

$$\frac{2}{\mathcal{C}\Gamma_{d,\rm cr}} = 1, \quad (38)$$

where

$$\Gamma_{d,\rm cr} = L^{-\frac{1}{3}}V_L l_{d,\rm cr}^{-\frac{2}{3}}. \quad (39)$$

It yields (XL16)

$$l_{d,\rm cr} = \left(\frac{\mathcal{C}}{2}\right)^{\frac{3}{2}}L^{-\frac{1}{2}}V_L^{\frac{3}{2}}. \quad (40)$$

By inserting the above expression in Equation (18), we obtain the timescale of the damping stage,

$$\tau_{\rm dam} = t(l_d = l_{d,\rm cr}) - t_1(l_{d1} = l_\nu) = \frac{23}{3}\left(\frac{\mathcal{C}}{2} - \Gamma_\nu^{-1}\right). \quad (41)$$

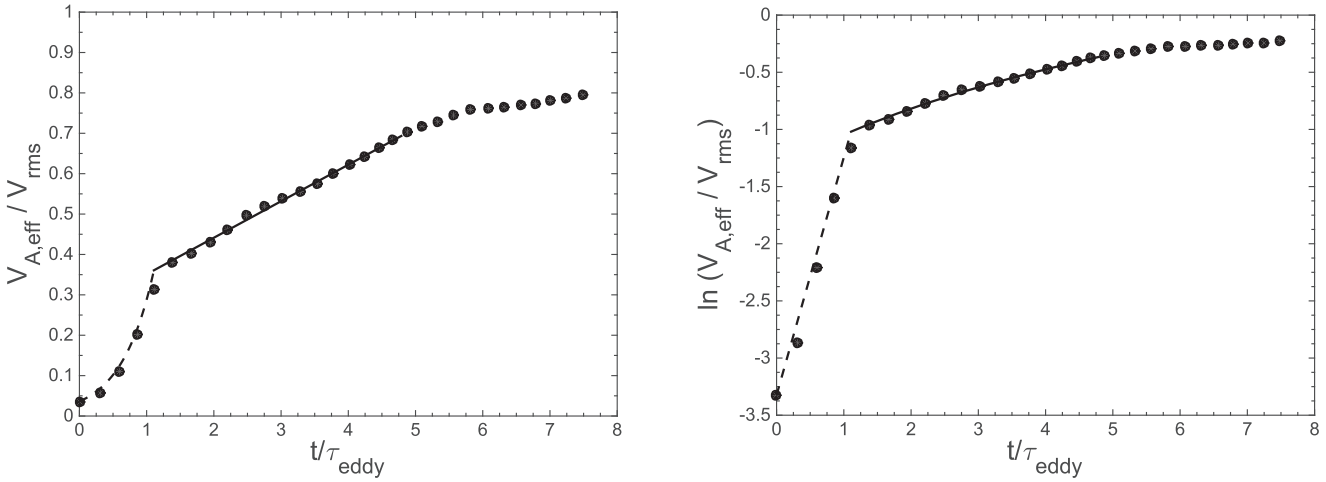

Figure 3. (a) Time evolution of the numerically measured $V_{A,\rm eff}$ (normalized by $V_{\rm rms}$, filled circles) in comparison with our theoretical prediction, where the dashed and solid lines represent the dissipation-free (Equation (29)) and damping (Equation (32)) stages of a dynamo, respectively. (b) Same as (a) but for the logarithm of $V_{A,\rm eff}/V_{\rm rms}$.

Here, we assume that the initial magnetic field is sufficiently weak and thus the damping stage starts from l_ν. The values of $l_{d,\rm cr}$ and $\tau_{\rm dam}$ for MC and DC are listed in Table 3.

At the end of the damping stage, $\mathcal{E}_M$ becomes

$$\mathcal{E}_{M,\rm dam}=\frac{1}{2}v_{d,\rm cr}^2=\frac{1}{2}V_L^2L^{-\frac{2}{3}}l_{d,\rm cr}^{\frac{2}{3}}. \quad (42)$$

By inserting Equation (40) into the above equation, we obtain (XL16)

$$\mathcal{E}_{M,\rm dam}=\frac{\mathcal{C}}{4}L^{-1}V_L^3, \quad (43)$$

which can also be derived by combining Equation (13) with Equation (40). The corresponding field strength is

$$B_{\rm dam}=\sqrt{8\pi\rho_{\rm eff}\mathcal{E}_{M,\rm dam}}. \quad (44)$$

According to Equation (38), the ion-neutral coupling becomes strong at the end of damping stage. By using $\rho_{\rm eff}=\rho$ in the above expression, we determine the values of $B_{\rm dam}$, as presented in Table 3. We see that due to the small length scale, the short timescale, and the resulting weak magnetic field, the damping stage is not important for the dynamo process induced by the interstellar turbulence in the partially ionized ISM.

After the short damping stage, the turbulent dynamo enters the nonlinear regime. Both the dynamo stretching and turbulent diffusion of magnetic fields mainly take place at l_p of $M(k, t)$, where (XL16)

$$\Gamma_p\mathcal{E}_M=\frac{1}{2}L^{-1}V_L^3. \quad (45)$$

By comparing $\omega_{\rm IN}$ at l_p with Γ_p (Equations (6) and (45)),

$$\frac{\omega_{\rm IN}(l=l_p)}{\Gamma_p}=\frac{\mathcal{C}l_p^{-2}\mathcal{E}_M}{\Gamma_p}=\frac{\mathcal{C}\Gamma_p}{2}, \quad (46)$$

we see that because *Condition (1)* breaks down in the nonlinear stage, the above ratio is less than unity. As the nonlinear turbulent dynamo is in a strongly coupled regime, the magnetic field diffusion due to the slippage between ions and neutrals and the ion-neutral collisional damping are unimportant for the nonlinear stage of a dynamo (XL16).

The nonlinear turbulent dynamo leads to a scale-by-scale equipartition between the turbulent energy and the magnetic energy. At the full saturation at L, all the turbulent energy carried by strongly coupled ions and neutrals can be converted to the magnetic energy. The saturated field strength $B_{\rm non}=\sqrt{4\pi\rho}V_L$ at the end of the nonlinear stage is presented in Table 3, which provides the maximum magnitude of turbulent magnetic fields in the partially ionized ISM. These estimates are also consistent with the Zeeman measurements by Crutcher et al. (2010). It implies that the nonlinear turbulent dynamo accounts for the turbulent magnetic fields observed in the ISM.

The timescale of the nonlinear stage is (XL16)

$$\tau_{\rm non}=\frac{19}{3}\left(\frac{L}{V_L}-\Gamma_\nu^{-1}\right) \quad (47)$$

in WNM and CNM, and

$$\tau_{\rm non}=\frac{19}{3}\left(\frac{L}{V_L}-\frac{\mathcal{C}}{2}\right). \quad (48)$$

in MC and DC (see Table 3). It is approximately $6\tau_{\rm eddy}$, which is longer than $\tau_{\rm dam}$ by several orders of magnitude.

(b) Preshock turbulence in SNRs.

When an SNR shock sweeps through the ISM, the preshock turbulence can be driven by the interaction between the cosmic-ray pressure gradient and interstellar density inhomogeneities (Beresnyak et al. 2009). We consider the driving condition to be (XL17)

$$L=0.1\ {\rm pc},\ \ V_L=10^3\ {\rm km\ s^{-1}}. \quad (49)$$

Here, we use the characteristic scale of the density structure in the cold ISM (Goodman et al. 1998; Heiles & Troland 2003) as L, and V_L is of the order of the shock velocity. With a high dynamo stretching rate and *Condition (1)* satisfied in the entire inertial range $[L, l_\nu]$ of preshock turbulence (see Figure 5(b)), the preshock turbulent dynamo in all partially ionized phases remains in the damping stage. $l_{d,\rm cr}$ in this case is equal to L.

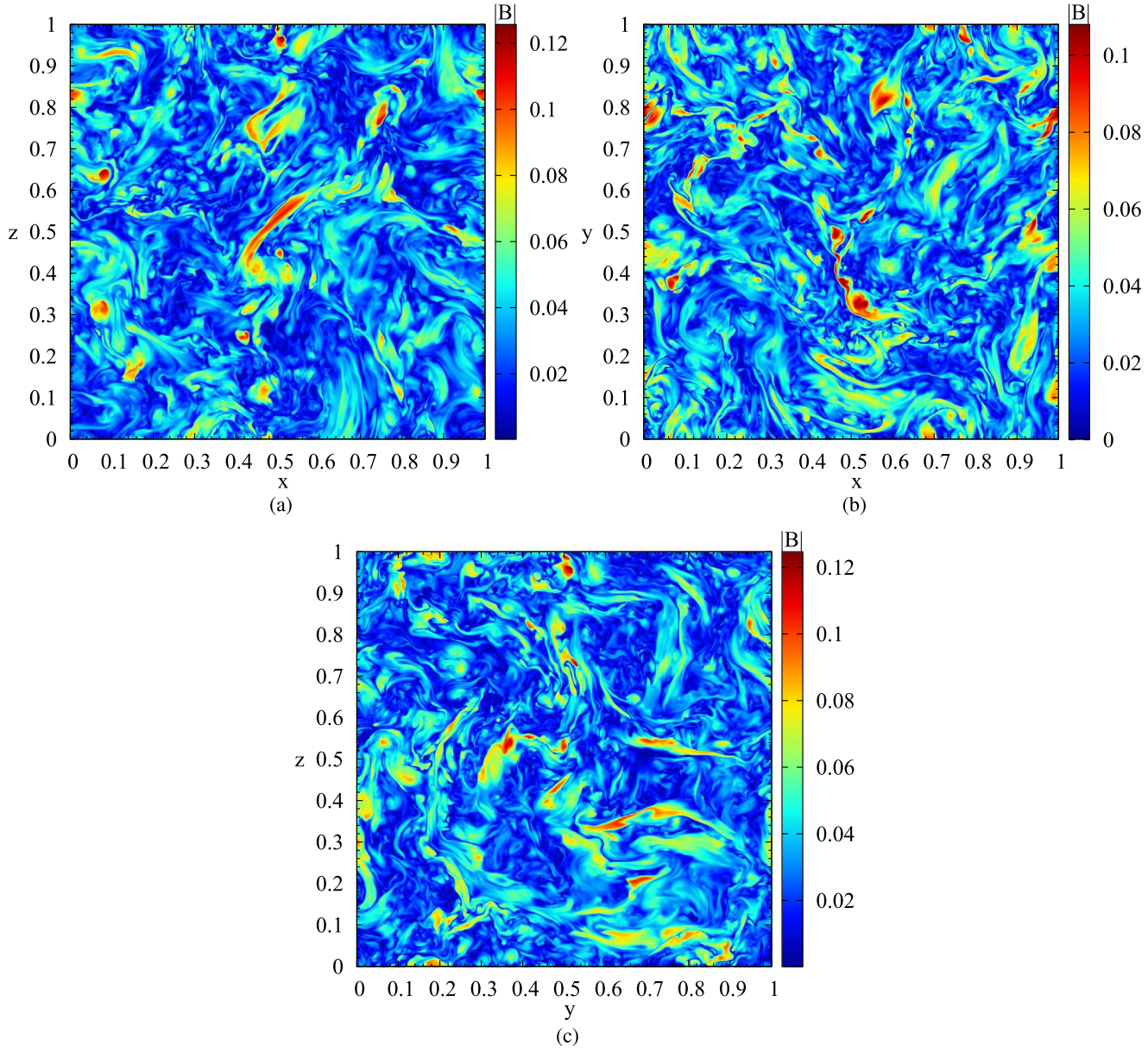

Figure 4. A 2D cross section through the middle of the computational domain of the numerically measured magnetic field strength in the (a) *xz* plane, (b) *xy* plane, and (c) *yz* plane, corresponding to $M(k, t)$ at $t = 7.49\ \tau_{\rm eddy}$ in Figure 2(a).

Accordingly, the damping stage has a timescale

$$\tau_{\rm dam} = t(l_d = L) - t_1(l_{d1} = l_\nu) = \frac{23}{3}\left(\frac{L}{V_L} - \Gamma_\nu^{-1}\right). \quad (50)$$

Here, we again assume that the dynamo starts at l_ν with sufficiently weak seed field. As $1/\Gamma_\nu$ is negligibly small compared with L/V_L, the values of $\tau_{\rm dam}$ in different phases are approximately the same (see Table 3). We note that $\tau_{\rm dam}$ is sufficiently small compared to the precursor crossing time $\tau_c \sim (c/v_{\rm sh})\ L/V_L$, where c and $v_{\rm sh}$ represent light speed and shock velocity, respectively (XL17). So the L-scale magnetic field can be amplified within τ_c.

$\mathcal{E}_{M,\rm dam}$ at the end of damping stage is given by Equation (21). As the damping stage of a dynamo is in a weakly coupled regime, we adopt $\rho_{\rm eff} \sim \rho_i$ and present $B_{\rm dam} \sim \sqrt{8\pi\rho_i \mathcal{E}_{M,\rm dam}}$ as the lower limit of $B_{\rm dam}$ in Table 3. The dynamo-amplified magnetic field can confine energetic particles near the shock to facilitate the shock acceleration. For example, the maximum energy of cosmic rays that can be confined by the resulting preshock magnetic field in the case of MC is

$$E_{\rm CR,max} = eB_{\rm dam}L = 38.4\ {\rm PeV}. \quad (51)$$

This already reaches the PeV knee of the cosmic-ray spectrum and supports the Galactic origin of the cosmic rays below the knee. Additionally, magnetic fields of the order of 100 μG near the shock front of SNRs are also inferred from observations (e.g., Bamba et al. 2003, 2005a, 2005b; Vink 2012).

5. Ion-neutral Coupling in MHD Turbulence and in a Turbulent Dynamo

In a partially ionized medium, the coupling state between ions and neutrals is crucial for determining the damping of MHD turbulence and the efficiency of a turbulent dynamo.

Table 3
Turbulent Dynamo in the Partially Ionized ISM

	WNM	CNM	MC	DC
$n_{\rm H}$ [cm^{-3}]	0.4	30	300	10^4
$n_e/n_{\rm H}$	0.1	10^{-3}	10^{-4}	10^{-6}
T [K]	6000	100	20	10
Interstellar turbulence				
$l_{d,\rm cr}$ [pc]	⋯	⋯	6.3×10^{-6}	3.3×10^{-5}
$\tau_{\rm dam}$ [kyr]	⋯	⋯	0.4	2.3
$B_{\rm dam}$ [μG]	⋯	⋯	0.5	4.7
$\tau_{\rm non}$ [kyr]	1.9×10^4	1.9×10^4	1.9×10^4	1.9×10^4
$B_{\rm non}$ [μG]	3.0	25.1	79.5	458.1
Preshock turbulence				
$l_{d,\rm cr}$ [pc]			0.1	
$\tau_{\rm dam}$ [kyr]			0.75	
$B_{\rm dam}$ [μG]	79.1	56.6	415.2	138.2

MHD turbulence. In the strong Alfvénic turbulence with the magnetic energy in equipartition with the turbulent energy at L, there is a *critical balance* between the turbulent cascade rate, i.e., eddy-turnover rate, $v_l/l_\perp$ and the Alfvén wave frequency $\omega_A = V_{A,\rm eff}/l_\parallel$ (Goldreich & Sridhar 1995), where $l_\perp$ and $l_\parallel$ are the perpendicular and parallel components of the length scale with respect to the *local* magnetic field (Lazarian & Vishniac 1999). The anisotropic scaling resulting from the *critical balance* in the *local* reference system has been confirmed in both one-fluid (e.g., Cho & Lazarian 2002, 2003) and two-fluid (Burkhart et al. 2015) MHD simulations down to the dissipation scale of Alfvénic turbulence.

The ion-neutral collisional damping of the turbulent cascade depends on the coupling state between ions and neutrals. As summarized in Table 4, in the low wave frequency range with $\omega_A < \nu_{ni}$, Alfvén waves with $V_{A,\rm eff} = V_{A,\rm tot}$ propagate in the strongly coupled ions and neutrals.[5] By contrast, at high wave frequencies with $\omega_A > \nu_{in}$, ions and neutrals are essentially decoupled from each other, and Alfvén waves with $V_{A,\rm eff} = V_{Ai}$ can only propagate in ions. Within intermediate wave frequencies, neutrals are decoupled from ions, but ions are still collisionally coupled to neutrals. Accordingly, Alfvén waves propagating in the weakly coupled ions and neutrals have (Xu et al. 2015, 2016)

$$\omega_A^2 = \frac{k_\parallel^2 V_{Ai}^2[(1+\chi)\nu_{ni}^2 + k_\parallel^2 V_{Ai}^2]}{(1+\chi)^2\nu_{ni}^2 + k_\parallel^2 V_{Ai}^2} = k_\parallel^2 V_{A,\rm eff}^2, \quad (52)$$

where $k = 1/l$, $\chi = \rho_n/\rho_i$, and

$$V_{A,\rm eff} = \sqrt{\frac{(1+\chi)\nu_{ni}^2 + k_\parallel^2 V_{Ai}^2}{(1+\chi)^2\nu_{ni}^2 + k_\parallel^2 V_{Ai}^2}}\, V_{Ai}, \quad (53)$$

which depends on the length scale. MHD turbulence in the weak coupling regime is subjected to the severest ion-neutral collisional damping. As a result, both Alfvén waves and Alfvénic turbulent motions are damped in the weak coupling regime.

[5] In the strong Alfvénic turbulence, Alfvén waves can only propagate over the distance of one wavelength due to their nonlinear interactions.

It is worth noting that the ambipolar diffusion scale frequently used in the literature (e.g., Mouschovias 1991)

$$l_{\rm AD} = \frac{V_{A,\rm tot}}{\nu_{ni}} \quad (54)$$

is only equivalent to the parallel neutral-ion decoupling scale for the anisotropic Alfvénic turbulence. Since the energy of Alfvénic turbulence cascades mainly along the direction perpendicular to the *local* magnetic field, we are concerned with the perpendicular neutral-ion decoupling scale, which is related to $l_{\rm AD}$ via the *critical balance* mentioned above.

Turbulent dynamo. Similarly, there also exist different ion-neutral coupling regimes for the turbulent dynamo, depending on the range of Γ_l (see Table 4). When $\Gamma_l < \nu_{ni}$, turbulence in the strongly coupled ions and neutrals induces the growth of magnetic energy, which can be expressed in terms of $V_{A,\rm eff} = V_{A,\rm tot}$. When $\Gamma_l > \nu_{in}$, neutrals are not involved in the dynamo process. The dynamo only operates in ions and results in the growth of magnetic energy in terms of $V_{A,\rm eff} = V_{Ai}$. For the intermediate Γ_l considered in this work, the dynamo takes place in the weakly coupled ions and neutrals and is affected by the strongest ion-neutral collisional damping. As a result, the dynamo has a damping stage.

Besides ion-neutral collisional damping, the viscosity in neutrals also leads to the damping of MHD turbulence in a partially ionized medium (Lazarian et al. 2004). The parameter space for the dominance of neutral viscous damping and the appearance of the new regime of MHD turbulence in the sub-viscous range (Cho et al. 2002a, 2003) is provided in Xu & Lazarian (2017b). In the context of a turbulent dynamo, the damping stage of a dynamo can only arise when the ion-neutral collisional damping is stronger than the neutral viscous damping.

6. Summary

We have studied the turbulent dynamo in a weakly ionized medium and numerically tested the damping stage of a dynamo as theoretically predicted by XL16. Here, we summarize our main results.

1. We have explicitly provided the physical conditions under which the damping stage of a dynamo can arise in a partially ionized medium. They are Equation (2) and Equation (9), and Equation (19) for the damping stage to persist until the damping scale reaches the injection scale L of turbulence. With a sufficiently small ionization fraction and seed magnetic field, the timescale of a damping stage is around eight times the largest eddy-turnover time (Section 2).
2. By performing a two-fluid dynamo simulation under the above conditions (Equations (2), (9), and (19)) and quantitative comparisons between the theoretical predictions and numerical measurements, we have numerically confirmed the linear-in-time growth of magnetic field strength due to the severe ion-neutral collisional damping in the damping stage of a dynamo. As a result of the weak coupling between ions and neutrals, most turbulent kinetic energy contained in neutrals cannot be converted to the magnetic energy (Section 3).
3. We have examined the physical conditions for the damping stage of a dynamo in the partially ionized ISM and provided the parameter space for its appearance

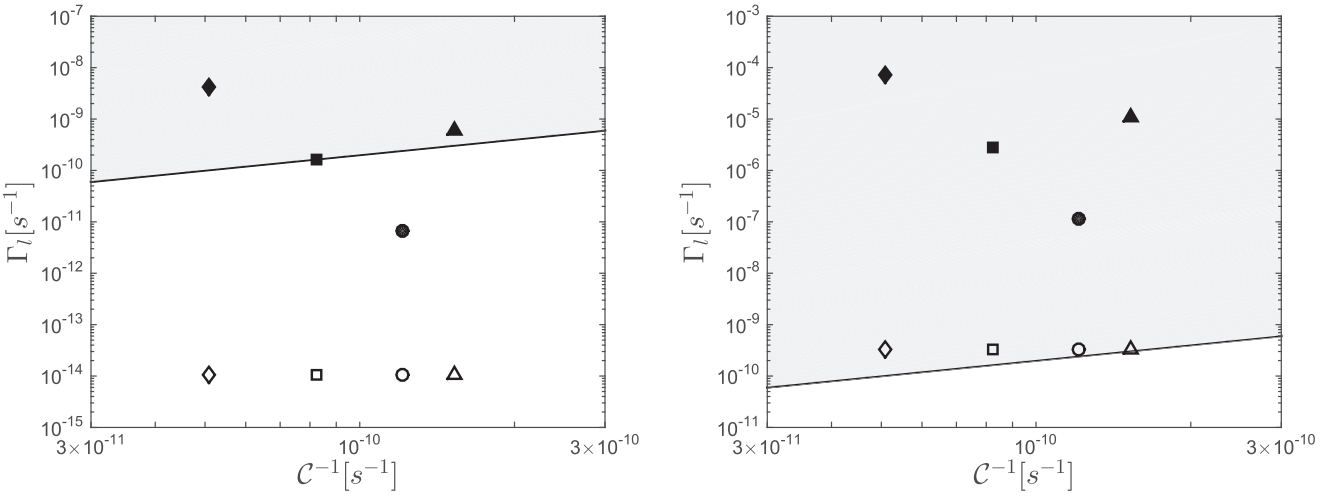

(a) Interstellar turbulence (b) Preshock turbulence

Figure 5. The shaded region shows the parameter space for the appearance of the damping stage of a dynamo. The symbols represent the values for WNM (circle), CNM (square), MC (triangle), and DC (diamond). The filled and open symbols correspond to Γ_ν and Γ_L, respectively.

Table 4
Ion-neutral Coupling in MHD Turbulence and Turbulent Dynamo

Coupling State	Strong Coupling	Weak Coupling	Decoupling
MHD turbulence	$\omega_A < \nu_{ni}$	$\nu_{ni} < \omega_A < \nu_{in}$	$\omega_A > \nu_{in}$
Turbulent dynamo	$\Gamma_l < \nu_{ni}$	$\nu_{ni} < \Gamma_l < \nu_{in}$	$\Gamma_l > \nu_{in}$

(Section 4). For the dynamo induced by the interstellar turbulence, the damping stage contributes insignificantly to the dynamo growth of magnetic energy. Instead, the nonlinear stage is mainly responsible for the growth of the interstellar turbulent magnetic fields. By contrast, the dynamo induced by the preshock turbulence in SNRs remains in the damping stage, which is important for studying the magnetic field amplification and cosmic-ray acceleration at shocks.

S.X. acknowledges the support for Program number *HST*-HF2-51400.001-A provided by NASA through a grant from the Space Telescope Science Institute, which is operated by the Association of Universities for Research in Astronomy, Incorporated, under NASA contract NAS5-26555. S.X. also thanks Chris McKee for useful conversations. D.S.B. acknowledges support via NSF grants NSF-ACI-1533850, NSF-DMS-1622457, NSF-ACI-1713765, and NSF-DMS-1821242. Support from a grant by Notre Dame International is also acknowledged. A.L. acknowledges the support from grant NSF-DMS-1622353.

ORCID iDs

Siyao Xu https://orcid.org/0000-0002-0458-7828

References

Balsara, D. S. 1996, ApJ, 465, 775
Balsara, D. S. 1998a, ApJS, 116, 119
Balsara, D. S. 1998b, ApJS, 116, 133
Balsara, D. S. 2004, ApJS, 151, 149
Balsara, D. S. 2010, JCoPh, 229, 1970
Balsara, D. S. 2012, JCoPh, 231, 7476
Balsara, D. S., & Spicer, D. 1999a, JCoPh, 148, 133
Balsara, D. S., & Spicer, D. S. 1999b, JCoPh, 149, 270
Bamba, A., Yamazaki, R., & Hiraga, J. S. 2005a, ApJ, 632, 294
Bamba, A., Yamazaki, R., Ueno, M., & Koyama, K. 2003, ApJ, 589, 827
Bamba, A., Yamazaki, R., Yoshida, T., Terasawa, T., & Koyama, K. 2005b, ApJ, 621, 793
Beresnyak, A. 2012, PhRvL, 108, 035002
Beresnyak, A., Jones, T. W., & Lazarian, A. 2009, ApJ, 707, 1541
Brandenburg, A., & Subramanian, K. 2005, PhR, 417, 1
Burkhart, B., Lazarian, A., Balsara, D., Meyer, C., & Cho, J. 2015, ApJ, 805, 118
Cho, J., & Lazarian, A. 2002, PhRvL, 88, 245001
Cho, J., & Lazarian, A. 2003, MNRAS, 345, 325
Cho, J., Lazarian, A., & Vishniac, E. T. 2002a, ApJL, 566, L49
Cho, J., Lazarian, A., & Vishniac, E. T. 2002b, ApJ, 564, 291
Cho, J., Lazarian, A., & Vishniac, E. T. 2003, ApJ, 595, 812
Cho, J., & Vishniac, E. T. 2000, ApJ, 538, 217
Cho, J., Vishniac, E. T., Beresnyak, A., Lazarian, A., & Ryu, D. 2009, ApJ, 693, 1449
Crutcher, R. M., Wandelt, B., Heiles, C., Falgarone, E., & Troland, T. H. 2010, ApJ, 725, 466
Downes, T. P. 2012, MNRAS, 425, 2277
Draine, B. T. 1986, MNRAS, 220, 133
Draine, B. T., & Lazarian, A. 1998, ApJL, 494, L19
Draine, B. T., Roberge, W. G., & Dalgarno, A. 1983, ApJ, 264, 485
Falkovich, G. 1994, PhFl, 6, 1411
Goldreich, P., & Sridhar, S. 1995, ApJ, 438, 763
Goodman, A. A., Barranco, J. A., Wilner, D. J., & Heyer, M. H. 1998, ApJ, 504, 223
Han, J. L. 2017, ARA&A, 55, 111
Haugen, N. E., Brandenburg, A., & Dobler, W. 2004, PhRvE, 70, 016308
Haugen, N. E. L., Brandenburg, A., & Dobler, W. 2003, ApJL, 597, L141
Heiles, C., & Troland, T. H. 2003, ApJ, 586, 1067
Kazantsev, A. P. 1968, JETP, 26, 1031
Kowal, G., Lazarian, A., Vishniac, E. T., & Otmianowska-Mazur, K. 2009, ApJ, 700, 63
Kowal, G., Lazarian, A., Vishniac, E. T., & Otmianowska-Mazur, K. 2012, NPGeo, 19, 297
Kulsrud, R. M., & Anderson, S. W. 1992, ApJ, 396, 606
Langer, W. D. 1978, ApJ, 225, 95
Lazarian, A., & Vishniac, E. T. 1999, ApJ, 517, 700
Lazarian, A., Vishniac, E. T., & Cho, J. 2004, ApJ, 603, 180
Li, P. S., McKee, C. F., Klein, R. I., & Fisher, R. T. 2008, ApJ, 684, 380
Lithwick, Y., & Goldreich, P. 2001, ApJ, 562, 279
Maron, J., & Blackman, E. G. 2002, ApJL, 566, L41
Maron, J., Cowley, S., & McWilliams, J. 2004, ApJ, 603, 569
Maron, J., & Goldreich, P. 2001, ApJ, 554, 1175
Meyer, C. D., Balsara, D. S., Burkhart, B., & Lazarian, A. 2014, MNRAS, 439, 2197
Mouschovias, T. C. 1991, ApJ, 373, 169
Oishi, J. S., & Mac Low, M.-M. 2006, ApJ, 638, 281

Schekochihin, A. A., Maron, J. L., Cowley, S. C., & McWilliams, J. C. 2002, ApJ, 576, 806
Shu, F. H. 1992, The Physics of Astrophysics, Vol. II, Gas dynamics (Mill Valley, CA: Univ. Science Books)
Spitzer, L. 1978, Physical Processes in the Interstellar Medium (New York: Wiley-Interscience)
Subramanian, K. 1998, MNRAS, 294, 718
Tilley, D. A., & Balsara, D. S. 2008, MNRAS, 389, 1058
Tilley, D. A., & Balsara, D. S. 2010, MNRAS, 406, 1201
Tilley, D. A., & Balsara, D. S. 2011, MNRAS, 415, 3681
Tilley, D. A., Balsara, D. S., & Meyer, C. 2012, NewA, 17, 368
Vink, J. 2012, A&ARv, 20, 49
Vranjes, J., & Krstic, P. S. 2013, A&A, 554, A22
Xu, S., & Lazarian, A. 2016, ApJ, 833, 215
Xu, S., & Lazarian, A. 2017a, ApJ, 850, 126
Xu, S., & Lazarian, A. 2017b, NJPh, 19, 065005
Xu, S., Lazarian, A., & Yan, H. 2015, ApJ, 810, 44
Xu, S., Yan, H., & Lazarian, A. 2016, ApJ, 826, 166
Zaqarashvili, T. V., Khodachenko, M. L., & Rucker, H. O. 2011, A&A, 529, A82